Biosensors and Bioelectronics 148 (2020) 111834

Contents lists available at ScienceDirect

Biosensors and Bioelectronics

journal homepage: http://www.elsevier.com/locate/bios

An enzyme-free electrochemical biosensor based on well monodisperse Au nanorods for ultra-sensitive detection of telomerase activity

Lei Wang, Tianjiao Meng, Dan Zhao, Huixian Jia, Siying An, Xinjian Yang, Huan Wang, Yufan Zhang *

Key Laboratory of Medicinal Chemistry and Molecular Diagnosis of the Ministry of Education, Key Laboratory of Analytical Science and Technology of Hebei Province, College of Chemistry and Environmental Science, Hebei University, 071002, Baoding, PR China

ARTICLE INFO

Keywords:
Telomerase activity
Electrochemical biosensor
Au nanorods
Ultra-sensitivity detecting

ABSTRACT

Efficient platforms for detecting telomerase activity are essential for early tumor monitoring and diagnosis. Herein, an enzyme-free electroanalytical strategy was developed for reliable and highly sensitive telomerase activity assay based on the increased electrochemical signals of methylene blue (MB) catalyzed by well monodisperse Au nanorods (AuNRs). In the presence of dNTPs and telomerase extracts, the assistant DNA 1 in the double stranded DNA can be extended to telomere repeat units $(TTAGGG)_n$, which could form a hairpin structure by telomerase-triggered extension. The assistant DNA 2 was ingeniously dissociated from the double stranded DNA to combine with capture DNA. As a result, a large amount of AuNRs could be anchored on the surface of these sequences and used for electrocatalytic oxidation of MB. The developed biosensor showed a low limit of detection of 8.20 HeLa cells mL^{-1} and a wide dynamic range from 30 to 1.04×10^7 HeLa cells mL^{-1} for the determination of telomerase activity, which can provide a new way for telomerase activity assays in early diagnosis for cancers.

1. Introduction

Telomerase is a ribonucleoprotein complex that extends a repetitive bases (TTAGGG) onto the 3′ ends of telomeres to maintain telomere length (Cohen et al., 2007; Stone et al., 2007). It has been regarded as a valuable biomarker for monitoring human malignant tumors. Substantial studies demonstrated the high telomerase activity expression in a majority of human cancer cells (~85%), while it exhibits activity depression in most normal somatic cells. Therefore, the sensitive evaluation of telomerase activity is very important for early diagnosis and treatment of tumors (Arndt and MacKenzie, 2016; Blackburn, 2001; Wang et al., 2016). Up to now, many efforts have been exerted to develop detection methods for telomerase activity. However, conventional techniques, such as surface enhanced Raman scattering (Ma et al., 2017; Shi et al., 2016), colorimetry (Xu et al., 2017; Zhang et al., 2016), and fluorescence (Gao et al., 2016; Yan et al., 2014), usually require tedious pretreatment, expensive instruments, and skilled technicians, restricting their applications. Although the telomere repeat amplification protocol (TRAP) is considered as a traditional approach for evaluating telomerase activity, it suffers from the inherent limitations such as unstable activity of enzymes and harsh reagent storage conditions (Kim et al., 1994; Xu, 2011; Zhou and Xing, 2012). Therefore, the development of reliable and sensitive strategies for telomerase activity assay is still highly desired. In comparison, electrochemical methods have received particular attention in analytical sensing of biological molecules, owing to its intrinsic advantages such as high sensitivity, simple operation, low cost, and fast response time (Alizadehghodsi et al., 2016; Ensafi. 2019; Chandra et al., 2016; Li et al. 2019b, 2019c; Liu et al., 2018; Meng et al., 2020; Wang et al. 2019b, 2019c; Yi et al., 2014). Qu's group developed an electrochemical biosensor for telomerase activity based on DNA metallization by highly characteristic solid-state electrochemical process (Wu et al., 2014). Li and co-workers constructed an electrochemical sensing platform for the detection of telomerase activity based on a spired DNA tetrahedron (Li et al., 2015). A sensitive electrochemical biosensing platform for telomerase activity assay based on methylene blue (MB) acting as a G-guadruplex probe was designed by Liu et al., (2017). Yang et al. developed a method by using electrochemical impedance spectroscopy for telomerase activity assay (Yang et al., 2011).

Au nanorods (AuNRs) are among the most commonly used quasi-

* Corresponding author. Tel./fax: +86 03125079403.
E-mail address: zyf@hbu.edu.cn (Y. Zhang).

https://doi.org/10.1016/j.bios.2019.111834
Received 22 August 2019; Received in revised form 18 October 2019; Accepted 30 October 2019
Available online 2 November 2019

one-dimensional materials. AuNRs are well known as an excellent electrochemical tag due to their excellent catalytic activity, strong adsorption capacity and good conductivity (Du et al., 2017; Li et al., 2019a; Saha et al., 2018; Wang et al., 2018c; Yang et al., 2012). AuNRs were regarded as an effective platform to examine biological molecules and exhibit great potential for the signal amplification of biosensing (Kumar et al., 2019). Ordered mesoporous carbon (OMC) has attracted much attention because of its unique physical and chemical properties (Kong et al., 2017; Meng et al., 2019; Ryoo et al., 1999; Wang et al. 2018d, 2019a; Zhang et al., 2015). The combination of large specific surface area and good stability makes OMC highly promising as a good platform for loading other species. Especially, the acid-functionalized OMC has rich –COOH sites on its surface, which can provide a strong support for binding with DNA by biochemical self-assembly process.

In the present study, an enzyme-free electroanalytical strategy was developed for reliable and highly sensitive telomerase activity assay based on the increased electrochemical signals of methylene blue catalyzed by well monodisperse Au nanorods (AuNRs). This proposed electrochemical biosensor shows high sensitivity with wide linear range for detecting telomerase activity, providing a promising avenue in the field of bioassays. Referring to its attractive analytical characteristics, this electrochemical biosensor provides a favorable analytical tool for the telomerase-related early monitoring and diagnosis of cancer.

2. Experimental

2.1. General

$HAuCl_4{\cdot}3H_2O$, $MgCl_2$, sucrose, tetrachloroauric acid, glycerol, Tris-(hydroxymethyl) aminomethane (Tris), Tween 20, bovine serum albumin (BSA), ethylene glycol bis(2-aminoethyl ether)-*N*,*N*,*N*,*N*-tetraacetic acid (EGTA), phenylmethylsulfonyl fluorid (PMSF), 3-[(3-cholamidopropyl) dimethylammonio]-1-propanseulfonic acid (CHAPS), tetraethyl orthosilicate (TEOS), silver nitrate ($AgNO_3$), ascorbic acid, 2-mercaptoethanol, and hexadecyl trimethyl ammonium bromide (CTAB) were obtained from Shanghai Macklin Biochemical Co. Ltd. All DNA sequences, *N*-hydroxysuccinimide (NHS), deoxynucleotide mixture (dNTPs), and hydrochloride (EDAC) were purchased from Sangon Biotechnology Ins. (Shanghai, China). MB, KCl, HNO_3, ethanol absolute, $NaBH_4$, and NaOH were purchased from Beijing Chemical Co. Ltd. Nanopure water was purified by a Millipore filtration system (>18 MΩ. cm). The oligonucleotides are:

cDNA:5′–NH_2–AAAAAAAAATTCCTAGACGCAGCCCCTAACCCTAA-CTAGGAA–SH–3′

aDNA1: 5′-GCAGCCCCTAACCCTAACCCTAAAATCCGTCGAGCAGAGTT-3′

aDNA2: 5′-GTTAGGGTTAGGGGCTGC-3′

2.2. Apparatus

The morphologies of the as-prepared samples were performed by transmission electron microscopy (TEM, Tecnai G2, FEI) and scanning electron microscopy (SEM, Philips XL-30 ESEM). Flourier-transform infrared (FT-IR) spectra were determined using a FT-IR spectrometer (Nicolet Magna 560). The UV/Vis absorption spectra of AuNRs were determined by an UV/Vis spectrophotometer (U2900, Hitachi, Japan). Dynamic light scattering (DLS) of AuNRs was obtained by a Nano-DLS system (Malvern Instruments). The zeta potentials of samples were obtained by a Nano-ZS system (Malvern Instruments). The 1% agarose gels were performed in Tris-Acetate EDTA buffer (TAE buffer) at 75 mV for 36 min, and then the gel imaging was performed by ChemiDoc XRS+ with Image Lab software (Bio-RAD). Electrochemical measurements were conducted via the AUTOLAB Electrochemical Workstation (Metrohm Instruments) with a three-electrodes testing system at 25 °C. A glassy carbon electrode (GCE) was used as the working electrode. A Pt wire and an Ag/AgCl were used as the auxiliary and reference electrodes, respectively.

2.3. Preparation of AuNRs

AuNRs nanoprobe were synthesized using a previously reported method with minor modifications (Yang et al., 2012). Briefly, a brownish red seed solution was obtained by mixing of CTAB (0.20 M, 0.20 mL), $HAuCl_4$ (0.50 mM, 0.20 mL), and ice-cold $NaBH_4$ reductant (0.01 M, 0.02 mL) with rapid stirring. A freshly mixed solution containing 1.50 mL of $HAuCl_4{\cdot}3H_2O$ (23 mM), 0.50 mL of ascorbic acid (0.08 M), 1.2 mL of $AgNO_3$ (4.00 mM), 20.00 mL of CTAB (0.20 M), and 20.00 mL of nanopure water was added into the above seed solution, followed by stirring until the solution color gradually changed within 20 min. During the synthesis process, the temperature of this growth medium was kept at 28–30 °C. The AuNRs were obtained by centrifugation at 12,500 rpm for 25 min.

2.4. Synthesis of OMC support

OMC support was prepared according to the reported literature (Kong et al., 2017; Meng et al., 2019; Ryoo et al., 1999; Wang et al. 2018d, 2019a; Zhang et al., 2015). The acid-functionalized OMC materials were synthesized as follows. 0.30 g OMC powders were dissolved in HNO_3 (1 M, 50.00 mL) for 6 h under 90 °C. Then, the mixture was centrifugated and washed with ethanol until the pH approximately close to 7.0. The acid-functionalized OMC materials were dried at 70 °C for 6 h.

2.5. Cell culture and telomerase extraction

HeLa (Human cervix adenocarcinoma), MDA-MB-231, A549, and MCF-7 cell lines were cultured in Dulbecco's Modified Eagle Medium (DMEM) medium supplemented with 10% fetal bovine serum, 100 U mL^{-1} of penicillin and 100 U mL^{-1} of streptomycin at 37 °C (5% CO_2). For the telomerase extraction reaction, 1.04×10^7 cells were collected and resuspended in 1.0 mL of ice-cold CHAPS lysis buffer, containing PMSF (0.1 mM), glycerol (10%), 2-mercaptoethano (5 mM), EGTA (1 mM), $MgCl_2$ (1 mM), Tris-HCl (10 mM, pH 7.5), CHAPS (0.5%), and stored in an EP tube (4 mL). The cell lines were incubated for 20 min on ice, followed by centrifugation at 12,500 rpm for 20 min to remove the useless precipitates. Without disturbing the pellet, the finally clean supernatant was transferred to a fresh EP tube carefully and stored at −80 °C before use.

2.6. Fabrication of the proposed electrochemical biosensor

Telomerase extracts solution (10 μL), aDNA1-aDNA2 duplex (10 μL), and 2 mM of dNTPs mixture containing TRAP buffer (0.1 mg/mL BSA, 1 mM EGTA, Tween 20, 63 mM KCl, 20 mM Tris-HCl and 1.5 mM $MgCl_2$) were incubated at 37 °C for 150 min to proceed the telomerase-triggered extension. The GCE (3 mm diameter) was polished carefully with Al_2O_3 powder (d = 50 nm), and cleaned by nanopure water. The acid-functionalized OMC (2 mg/mL, 5 μL), prepared as described above, was dropped onto the surface of GCE. After drying at room temperature, NHS and EDC (10 mg/mL, 20 μL) were added onto the pretreated electrode surface. This modified electrode was then exposed to the cDNA (0.5 μM) in Tris-HCl buffer solution (10 mM, pH = 7.4) through amidation reaction and π-π stacking interaction. Telomerase extracts solution (10 μL), aDNA1-aDNA2 duplex (10 μL), and 2 mM of dNTPs mixture including TRAP buffer (0.1 mg/mL BSA, 1 mM EGTA, Tween 20, 63 mM KCl, 20 mM Tris-HCl and 1.5 mM $MgCl_2$) were incubated at 37 °C for 150 min to proceed the telomerase-triggered extension. Subsequently, the resulting electrode was incubated at 37 °C for 50 min with the telomerase extracts. Thereafter, 10 μL of AuNRs (2 mg/mL) were dropped onto the surface of modified electrode and further incubated at 37 °C for 50 min. Through this step, these monodisperse AuNRs were immobilized on sulfhydryl group at cDNA via a S–Au bond. The telomerase activity is related to the amount of the adsorbed electrocatalyst,

leading to the different electrochemical signals for readout. Scheme 1 demonstrates the principle of the strategy for detecting telomerase activity. For the electrochemical assay, the differential pulse voltammetry (DPV) was employed in PBS solution (0.1 M, pH = 7.4) with potential range from −0.5 to 0 V; interval time of 0.5 s; modulation time of 0.05 s; step potential of 5 mV; modulation amplitude of 25 mV.

3. Results and discussion

3.1. Characteristics of the as-prepared AuNRs and OMC

To characterize the morphologies of the as-prepared AuNRs, different methods were used. The TEM image of AuNRs electrocatalyst shown in Fig. 1A exhibits that the rod-like AuNRs have a mean length of 30.6 nm as well as a mean width of 7.9 nm with highly uniform size. UV–vis spectrophotometry shows that AuNRs with aspect ratio of approximately 3.8 is rod-shape structure (Fig. S1), which is consistent with the TEM result. Moreover, by counting from the high-resolution TEM image, the lattice fringe exhibits an interplanar spacing of 0.23 nm attributed to the face-centered cubic structure (111) of AuNRs (Fig. S2). The low-resolution morphology of AuNRs is shown in Fig. S3. Meanwhile, as revealed by DLS method (Fig. 1B), AuNRs exhibit the size of about 31 nm, which is in accord with the TEM result. The photos of AuNRs electrocatalyst solution are also shown in the inset of Fig. 1B.

Fig. S4A shows the SEM image of OMC with wormlike morphology. The OMC materials are made of short sticks with a length of about 1.5 μm. From the planar TEM image (Fig.S4B), the bright contrast strips display the pore-walls and these dark contrast cores represent empty channels. Moreover, the cross-sectional TEM image of OMC materials shows the uniform mesopores with highly hexagonal arrays (Fig.S4C).

Fig. S5 shows the FT-IR spectrum of acid-functionalized OMC sample. It evidently exhibits four main characteristic peaks centered around 1716, 1565, 1401 and 1259 cm^{-1}, respectively. The peak at 1401 cm^{-1} comes from aromatic C═C bonds. The peaks at 1716 and 1565 cm^{-1} can be assigned to C═O stretching bands and that at 1259 cm^{-1} can be assigned to C–O stretching band from carboxylic acid.

The zeta potentials of the as-prepared electrocatalyst were also analyzed and the results are shown in Fig. S6. Initially, the pure AuNRs, which were prepared by reduction of $HAuCl_4$ using ascorbic acid as reductant in the presence of $AgNO_3$ and CTAB surfactant, were positively charged. After being incubated with cDNA, the zeta potential decreased from 51.32 to −24.89 mV, which could guarantee their high adsorption. The zeta potential technique provides potent evidence for the successful junction of AuNRs-cDNA.

The effect of different concentrations of the AuNRs was studied by DPV measurements. As shown in Fig. S7, the electrochemical signals in response to different concentrations of AuNRs were studied. The AuNRs (2 mg/mL) performed the best electrocatalytic activity towards MB oxidation among the synthesized different concentrations of AuNRs. Thus, we focused on the fabrication of this biosensor with the concentrations of AuNRs of 2 mg/mL.

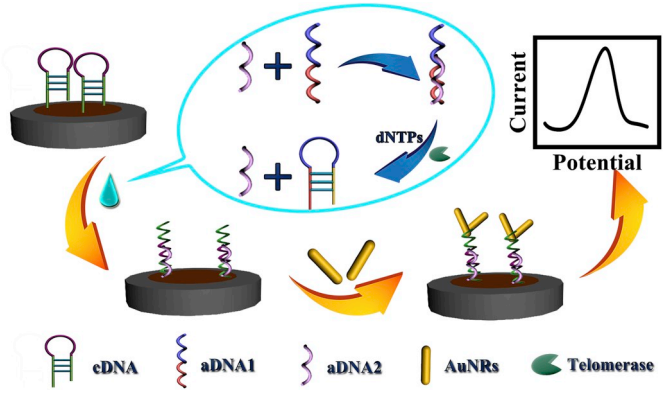

Scheme 1. A principle of electroanalytical method for the detection of telomerase activity.

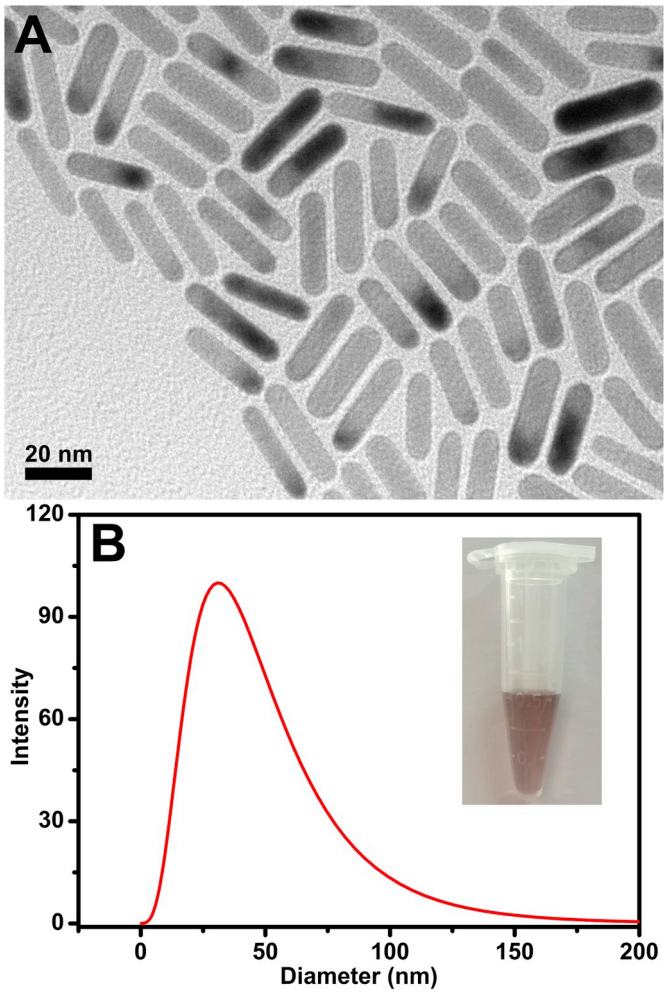

Fig. 1. TEM image of monodisperse AuNRs (A). DLS of AuNRs (B); inset: photographs of AuNRs solution.

3.2. Polyacrylamide gel electrophoresis characterization of the design strategy

In order to further verify the feasibility of the strategy, the polyacrylamide gel electrophoresis (PAGE) was employed. As shown in Fig. S8, cDNA (lane a), aDNA1 (lane b), aDNA2 (lane c), and aDNA1-aDNA2 duplex (lane d) exhibited a distinct single band. After mixing aDNA1-aDNA2 and cell extract, there appeared new bands in the top of lane e, suggesting the generation of the products of telomerase extension. Furthermore, after the incubation of aDNA1-aDNA2 was mixed with cell extract and cDNA, and the new bands appeared due to the formation of composite (lane f). Lane g shows the mixture of cDNA and aDNA1. After the aDNA2 was incubated with cDNA, the bright band was observed on the lane h, suggesting that aDNA2 was hybridized with cDNA. These observations strongly indicated that the designed sensing process was reasonable.

3.3. Design and electrochemical characterization of the biosensor

Electrochemical impedance spectroscopy (EIS) technique was utilized to investigate the interface performance of the different modified electrodes (Fig. 2). Moreover, the charge transfer resistance (R_{ct}) values

were measured by the Nyquist plot (Table S1). Compared with the bare GCE (curve a), OMC/GCE (curve b) shows a small semicircle part at high frequency due to the excellent conductivity of OMC material. The cDNA absorbed on OMC through amidation reaction and π-π stacking interaction. The value of R_{ct} increased for cDNA-OMC/GCE (curve c), suggesting the association of the cDNA sequences with OMC. On the other hand, after the interaction of the double stranded aDNA1+aDNA2 with telomerase extracts in the presence of dNTPs and the telomerase-triggered extension reaction, the aDNA1 in duplex was extended $(TTAGGG)_n$ to form a hairpin structure leading to aDNA2 dissociates from the double stranded DNA. The hairpin structure of the cDNA can be opened to form a double helix structure with aDNA2. Thus, the obtained modified electrode was named as aDNA2-cDNA-OMC/GCE and showed largest semicircle diameter at high frequencies (curve d). The value of R_{ct} increased in turn from curves a to d due to high resistance density of DNA. Because the sulfhydryl groups are exposed at its 3' end of opened cDNA, these monodisperse AuNRs are associated with cDNA sequences by Au–S bond formation. Moreover, the AuNRs-aDNA2-cDNA-OMC/GCE shows the significantly decreased resistance resulting in good conductivity of AuNRs.

The DPV technique was used to demonstrate the electrochemical performance of different electrodes for MB in Fig. 3A. Compared with the bare GCE (curve a), OMC/GCE (curve b) exhibits a larger electrocatalytic oxidation current due to the facilitated charge-transfer process on OMC material. The oxidation peaks decreased after the modified GCE was immersed in cDNA (curve c) and further mixed with the released aDNA2 (curve d) because of the high resistance density of DNA sequences, and this indicates the viability of biological self-assembly design. Interestingly, after bonding with AuNRs, this proposed electrochemical sensing platform shows obvious increased response current owing to the excellent electrocatalytic activity of AuNRs (curve e). These results confirmed the successful construction of the proposed electrochemical biosensor. Besides, the electrochemical biosensor showed a little electrochemical response signal in the absence of telomerase, which was attributed to the non-specific adsorption of AuNRs (Fig. S9).

The catalytic rate constant (k_{cat}) can be evaluated according to the equation:

$$\frac{I_{cat}}{I_L} = (\pi k_{cat} ct)^{1/2}$$

Where I_L is limited current in the absence of MB, I_{cat} is the catalytic current of MB at the surface of modified electrode, t is time elapsed (s) and c is the bulk concentration. The value of k_{cat} can be simply

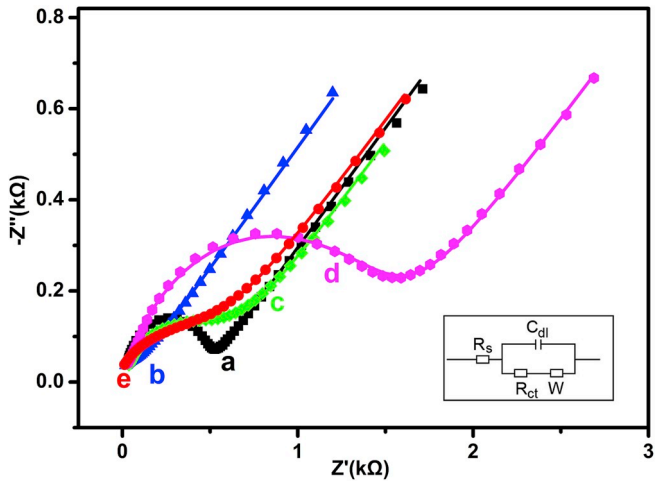

Fig. 2. EIS curves of the bare GCE (a), OMC/GCE (b), cDNA-OMC/GCE (c), aDNA2-cDNA-OMC/GCE (d), and AuNRs-aDNA2-cDNA-OMC/GCE (e); solution: $K_3Fe(CN)_6/K_4Fe(CN)_6$ (5.0 mM).

calculated from the inset (a) of Fig. S10 and the resulting value equals to 1979.08 $M^{-1}s^{-1}$. The diffusion coefficient (D) can also be determined based on the Cottrell equation:

$$I = nFAD^{1/2}c\pi^{-1/2}t^{-1/2}$$

where I refers to the peak current (A), A is the effective surface area of the electrode (cm^2), n is the total number of electron transferred ($n = 1$), c is the concentration of MB (mol mL^{-1}), and D is the diffusion coefficient (cm^2s^{-1}). The D was calculated to be 8.34×10^{-7} cm^2s^{-1} in the inset (b) of Fig. S10.

CV curves at various scan rates (v) were also studied. The anodic peak current (I_{pa}) increases linearly with ν (Fig. S11A), indicating that the redox reaction is a surface controlled reversible process. As shown in Fig. S11B, ΔE_P showed linear dependence vs. logν when the scan rate was larger than 100 mV/s. The relationship between ΔE_P and logν was described according to the Laviron's equation:

$$\Delta E_P = \frac{2.3RT}{(1-\alpha)\alpha nF} \times \left[\alpha log(1-\alpha) + (1-\alpha)log\alpha - log\left(\frac{RT}{nF}\right) - logk\right] + \frac{2.3RT}{(1-\alpha)\alpha nF} logv$$

where k is the heterogeneous electron transfer rate constant and α is the electron-transfer coefficient. The n was calculated to be 1.

3.4. Optimization of the related conditions

To attain the best optimized experimental conditions of this electrochemical biosensing platform, necessary conditions including the concentrations of cDNA and assistant DNA in duplex, as well as the incubation time, hybridization time, and modification time were favorably optimized. As shown in Fig. 3B, a rapidly increase in the response current was observed from 0 to 0.5 μM with the increase of cDNA concentrations and then tended to decrease, suggesting that the big amount of DNA sequences may produce steric hindrance on the electrode surface. Therefore, 0.5 μM of cDNA was selected as optimal concentration of cDNA. Fig. 3C shows that DPV peak current intensities increase with the increase of double stranded DNA (aDNA1-aDNA2) concentrations, but there was almost no change over 1.5 μM. Thus, 1.5 μM of aDNA1-aDNA2 duplex was an optimum concentration. The effect of incubation time for telomerase-triggered extension is shown in Fig. 3D. From this figure, it is clearly seen that the DPV peak currents response increased rapidly with increase of incubation time and reached a stable value at 150 min, due to the extension of telomerase-triggered extension. Therefore, the optimized incubation time used for electrode modification was 150 min. In addition, Fig. 3E exhibits the relation of the hybridization time between telomere repeats and aDNA1-aDNA2 duplex. The DPV response increased with the increase of hybridization time and reached plateau at 70 min. The modification time of AuNRs was also optimized. Obviously, a sharp DPV signal response increase was observed with the increase of modification time and reached a maximum signal at 50 min (Fig. 3F). So, the AuNRs modification time of 50 min was chosen as optimum modification time in the strategy.

3.5. Electroanalytical technique for telomerase activity assay

DPV measurements were carried out for detecting telomerase activity with different numbers of HeLa cells under the optimal conditions (the active telomerase extension product corresponding to different HeLa cell numbers). The electrochemical biosensing platform was constructed for reliable telomerase activity assay by using the increased response signals of MB electrocatalyzed by AuNRs. As presented in Fig. 4A, the DPV response curves increased with the increasing concentrations of HeLa cells. In the biological self-assembly design, (aDNA1+aDNA2) duplex can be extended to $(TTAGGG)_n$ to form a hairpin structure in aDNA1 due to the telomerase-triggered extension,

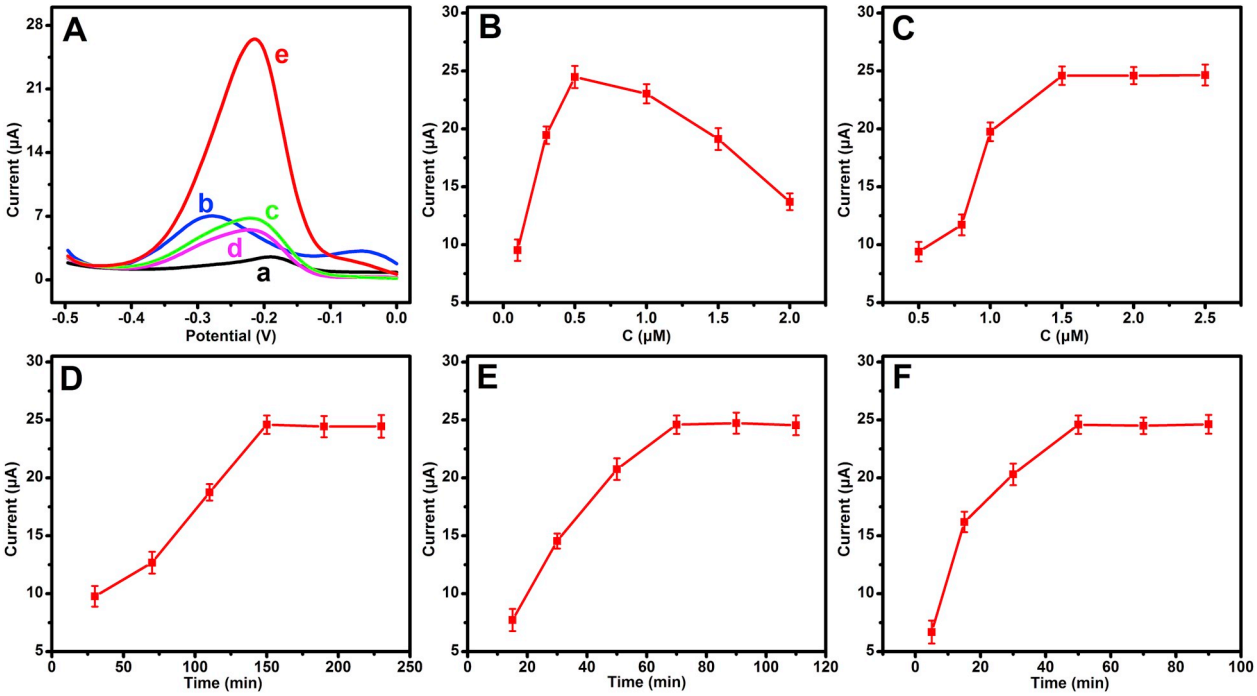

Fig. 3. DPV signals of the bare GCE (a), OMC/GCE (b), cDNA-OMC/GCE (c), aDNA2-cDNA-OMC/GCE (d), and AuNRs-aDNA2-cDNA-OMC/GCE (e) containing 20 μM of MB (A). Influence of the concentrations of cDNA (B) and aDNA1-aDNA2 duplex (C), incubation time for telomerase-triggered extension (D), hybridization reaction time between aDNA1-aDNA2 duplex and telomere repeats (E), modification time of AuNRs (F) on the DPV signals towards telomerase activities (the telomerase extracts were equivalent to 1×10^5 cells).

leading to aDNA2 dissociates from the double stranded DNA. Then, the hairpin structure of the cDNA can be opened to form a double helix structure with the released aDNA2, resulting in the exposure of the sulfhydryl groups at its 3' end of cDNA. Next, these cDNA sequences can be associated with monodisperse AuNRs nanoprobe, through Au–S bond formation, leading to the enhanced electrocatalytic current response signals towards MB. Telomerase activity can be expressed by HeLa cells numbers. With the increase of telomerase extension product, the more aDNA2 was released from double-stranded DNA, resulting in more cDNA bonded with AuNRs electrocatalyst. Therefore, the telomerase activity can be demonstrated by the electrocatalytic response signals. As presented in the inset of Fig. 4A, the electrochemical signals increased with increasing concentrations of HeLa cells and presented a strong correlation between the electrochemical response and the logarithm (log) of cells concentrations in the range from 30 to 1.04×10^7 HeLa cell mL^{-1}. The limit of detection was calculated as 8.20 HeLa cell mL^{-1}. These electroanalytical parameters of the proposed biosensor were compared with the other reported methods (Table 1). Compared with our reported method for telomerase activity detection, this method shows several distinct advantages. Firstly, the assistant DNA 2 were ingeniously dissociated from the double stranded DNA to combine with capture DNA, favoring anchoring of a large amount of AuNRs on the surface of these sequences. Meanwhile, it has a lower limit of detection. Additionally, the operation of the development of electrochemical biosensor for reliable and highly sensitive telomerase activity assay by well monodisperse Au nanorods was simple. Based on the attractive analytical characteristics, this electrochemical biosensor provides a favorable analytical tool for the telomerase-related early monitoring and diagnosis of cancer.

To evaluate the universality of the proposed strategy for telomerase activity assay, different cell lines extracts such as MCF-7, A549, and MDA-MB-231 were tasted (Fig. 4B). These telomerase activities of cell lines and heated cells were normalized to HeLa cells. As expected, all of the cell lines exhibited significantly amplified signals, demonstrating their positive telomerase activities. Contrarily, the weak electrochemical signals were observed for the heated cell extracts due to their loss of telomerase activities. These results clearly indicate that this method is adequate for expression levels of telomerase activity among different human cancer cells. Moreover, the Phi 29 DNA polymerase (Phi 29), T4 DNA ligase (T4), and T7 RNA polymerase (T7) were used as controls to evaluate the selectivity of the proposed method. Compared with telomerase, Phi 29, T4, and T7 showed small positive signal (Fig. S12). Thus, these results indicated that the proposed method has high selectivity for the detection of telomerase activity.

3.6. Stability, repeatability and real sample analysis

When the biosensor was stored in the fridge at 4 °C for two weeks, the DPV response signals remained at 97.95% of its initial value. Besides, the stability of the electrochemical biosensor was also studied on the scan rates of 200 mV/s. The electrochemical signal intensity remained at 97.80% of its initial value, suggesting a good stability of this proposed biosensor. In addition, the repeatability of the electrochemical biosensor for the detection of telomerase activity with ten electrodes was investigated. The obtained relative standard deviation (RSD) of 0.77%, 0.97%, 0.98% were corresponding to the repetitive tests of 7×10^3, 1×10^5, and 5×10^6 HeLa cell numbers, respectively. The result indicates that this electrochemical sensing platform has good repeatability.

To further investigate the practicability of this electrochemical biosensing platform, the proposed biosensor for telomerase activity assay was tested in human serum samples. The analytical characteristics are shown in Table S2. The average recoveries were obtained within the range of 96.7%–101.1%, which indicating that the proposed biosensor for the detecting telomerase activity has good practicability in real samples.

4. Conclusions

In summary, a novel electrochemical biosensor was fabricated for

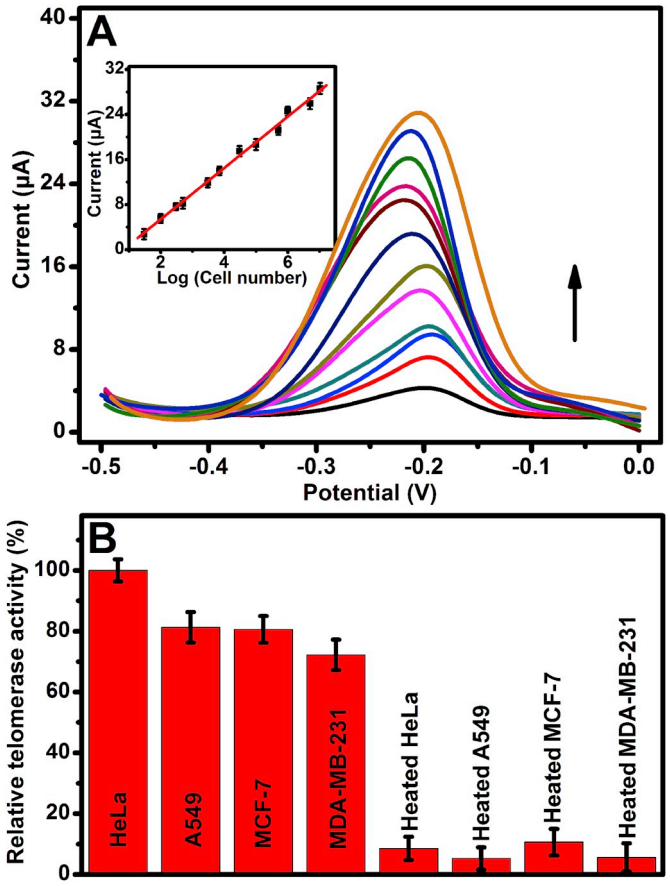

Fig. 4. DPV signals for readout in different Hela cell numbers (from top to bottom): 1.04×10^7, 5×10^6, 1×10^6, 5×10^5, 1×10^5, 3×10^4, 7×10^3, 3×10^3, 5×10^2, 3×10^2, 1×10^2, 3×10^1 (A). Electroanalytical technique to evaluate telomerase activities from different tumor cell extracts (B); these cell extracts were equivalent to 1×10^4 cells.

reliable and highly sensitive telomerase activity assay by using the increased response signals of MB electrocatalyzed by AuNRs signal nanoprobe. The feasibility of the designed strategy was investigated by using HeLa cells as the model, and directly monitoring the dose-dependent change in telomerase extracts (HeLa cell numbers) in response to the electrocatalytic response signals. To attain the best analytical performance of this electrochemical biosensing platform, some experimental conditions including the concentration of cDNA and assistant DNA in duplex, as well as the incubation time, hybridization time, and modification time were optimized. The developed enzyme-free electrochemical biosensor showed excellent electroanalytical parameters, providing a powerful and successful platform for ultra-sensitive determination of telomerase activity. Moreover, telomerase activities of different cancer cell lines were also favorably tested. This strategy may provide a new way in the biochemical assay for the detection of telomerase activity.

Declaration of competing interest

The authors declare that they have no known competing financial interests or personal relationships that could have appeared to influence the work reported in this paper.

CRediT authorship contribution statement

Lei Wang: Investigation, Methodology, Writing - original draft. **Tianjiao Meng:** Methodology, Software. **Dan Zhao:** Investigation, Software. **Huixian Jia:** Data curation, Writing - original draft. **Siying An:** Methodology, Data curation. **Xinjian Yang:** Software, Funding acquisition. **Huan Wang:** Writing - review & editing, Funding acquisition. **Yufan Zhang:** Investigation, Methodology, Data curation, Software, Supervision, Funding acquisition.

Table 1
Comparison between the proposed strategy and other methods for telomerase activity assay.

Strategy	Detection mode	Linear range	Limit of detection	Ref.
Difunctional Au NPs	UV–vis	6×10^3–9.4×10^4 HeLa cells mL^{-1}	6000 HeLa cells mL^{-1}	Duan et al. (2014)
G-quardruplex/ hemin controlled Au NPs	UV–vis	2.7×10^4–1.9×10^5 HeLa cells mL^{-1}	2.7×10^4 HeLa cells mL^{-1}	Sharon et al. (2014)
Bifunctionalized luminal-Au NPs	ECL	100–9×10^3 HeLa cells	62 HeLa cells	Zhang et al. (2014b)
Multifunctional Au NPs-based ECL sensor	ECL	313–1×10^4 HeLa cells	148 HeLa cells	Zhang et al. (2014a)
Hemin-graphene conjugates biosensor	Colorimetry	100–2×10^4 HeLa cells mL^{-1}	60 HeLa cells	Xu et al. (2017)
Via enzymatic etching of Au nanorods assay	Colorimetry	200–1.5×10^4 HeLa cells mL^{-1}	90 HeLa cells	Yang et al. (2017a)
Via CHA and etching of AuNRs	Colorimetry	20–5×10^2 HeLa cells	15 HeLa cells	Wang et al. (2018a)
Via monitoring urease regulated pH change	Colorimetry	50–1×10^4 HeLa cells	20 HeLa cells	Wang et al. (2018b)
Via DNAzyme and a hairpin shaped probe	Fluorescence	200–1×10^5 HeLa cells	200 HeLa cells	Tian et al. (2013)
Förster resonance energy transfer	Fluorescence	50–1×10^3 HeLa cells	33 HeLa cells	Yang et al. (2017b)
DNA self-assenbly technology	Fluorescence	50–2×10^3 HeLa cells	30 HeLa cells	Zhu et al. (2018)
AIEgens-based bioprobe with two fluorescent signals	Fluorescence	0–2×10^4 HeLa cells	250 HeLa cells	Zhuang et al. (2017)
Biosensor based on electrocatalysis of Au@CeMOF and conformation switch of hairpin DNA	SWV	200–2×10^6 HeLa cells	27 HeLa cells mL^{-1}	Dong et al. (2019)
Biosensor based on AuNRs-3 composite	DPV	100–1.04×10^7 HeLa cells mL^{-1}	52.81 HeLa cells mL^{-1}	Wang et al. (2019c)
Structure-switching DNA-based biosensor	DPV	100–6×10^4 HeLa cells mL^{-1}	100 HeLa cells mL^{-1}	Yi et al. (2014)
Electrochemical biosensor based on AuNRs	DPV	300–1.04×10^7 HeLa cells mL^{-1}	8.20 HeLa cells mL^{-1}	This work

Acknowledgements

The authors gratefully acknowledge the support from the Priority

Strategy Project of Key Laboratory of Medicinal Chemistry and Molecular Diagnosis of Ministry of Education (No. ts2019003), the Natural Science Foundation of Hebei Province (No. B2019201407, No. B2018201214, and No. B2018201221) and the Advanced Talents Incubation Program of the Hebei University (No.801260201026 and No. 801260201023).

Appendix A. Supplementary data

Supplementary data to this article can be found online at https://doi.org/10.1016/j.bios.2019.111834.

References

Alizadehghodsi, M., Zavarinematabad, A., Hamishehkar, H., Akbarzadeh, A., Mahmoudibadiki, T., Zarghami, F., Pourhassan, M.M., Alipour, E., Zarghami, N., 2016. Biosens. Bioelectron. 80, 426–432.
Arndt, G.M., MacKenzie, K.L., 2016. Nat. Rev. Cancer 16, 508.
Blackburn, E.H., 2001. Cell 106, 661–673.
Chandra, D.P., 2016. Nanobiosensors for Personalized and Onsite Biomedical Diagnosis, pp. 1–617.
Cohen, S.B., Graham, M.E., Lovrecz, G.O., Bache, N., Robinson, P.J., Reddel, R.R., 2007. Science 315, 1850–1853.
Dong, P., Zhu, L., Huang, J., Ren, J., Lei, J., 2019. Biosens. Bioelectron. 138, 111313.
Du, X., Dai, L., Jiang, D., Li, H., Hao, N., You, T., Mao, H., Wang, K., 2017. Biosens. Bioelectron. 91, 706–713.
Duan, R., Wang, B., Zhang, T., Zhang, Z., Xu, S., Chen, Z., Lou, X., Xia, F., 2014. Anal. Chem. 86, 9781–9785.
Ensafi, A.A., 2019. In Electrochemical Biosensors. Elsevier, pp. 1–373.
Gao, Y., Xu, J., Li, B., Jin, Y., 2016. Biosens. Bioelectron. 81, 415–422.
Kim, N.W., Piatyszek, M.A., Prowse, K.R., Harley, C.B., West, M.D., Ho, P.L., Coviello, G. M., Wright, W.E., Weinrich, S.L., Shay, J.W., 1994. Science 266, 2011–2015.
Kong, X., Wang, Y., Zhang, Q., Zhang, T., Teng, Q., Wang, L., Wang, H., Zhang, Y., 2017. J. Colloid Interface Sci. 505, 615–621.
Kumar, A., Purohit, B., Maueya, P.K., Pandey, L.M., Chandra, P., 2019. Electroanalysis 31, 1615–1629.
Li, F., Li, R., Feng, Y., Gong, T., Zhang, M., Wang, L., Meng, T., Jia, H., Wang, H., Zhang, Y., 2019. Mater. Sci. Eng. C 95, 78–85.
Li, M., Dong, P., Zhang, Y., 2019. J. Alloy. Compd 810, 151927.
Li, M., Yang, J., Lu, M., Zhang, Y., Bo, X., 2019. J. Colloid Interface Sci. 555, 449–459.
Li, Y., Wen, Y., Wang, L., Liang, W., Xu, L., Ren, S., Zou, Z., Zuo, X., Fan, C., Huang, Q., 2015. Biosens. Bioelectron. 67, 364–369.
Liu, X., Wei, M., Xu, E., Yang, H., Wei, W., Zhang, Y., Liu, S., 2017. Biosens. Bioelectron. 91, 347–353.
Liu, T., Li, M., Dong, P., Zhang, Y., Guo, L., 2018. Sens. Actuators, B 255, 1983–1994.
Ma, W., Fu, P., Sun, M., Xu, L., Kuang, H., Xu, C., 2017. J. Am. Chem. Soc. 139, 11752–11759.
Meng, T., Wang, L., Jia, H., Gong, T., Feng, Y., Li, R., Wang, H., Zhang, Y., 2019. J. Colloid Interface Sci. 536, 424–430.
Meng, T., Jia, H., Ye, H., Zeng, T., Yang, X., Wang, H., Zhang, Y., 2020. J. Colloid Interface Sci. 560, 1–10.
Ryoo, R., Joo, S.H., Jun, S., 1999. J. Phys. Chem. B 103, 7743–7746.
Saha, P., Hill, J.W., Walmsley, J.D., Hill, C.M., 2018. Anal. Chem. 90, 12832–12839.
Sharon, E., Golub, E., Niazov-Elkan, A., Balogh, D., Willner, I., 2014. Anal. Chem. 86, 3153–3158.
Shi, M., Zheng, J., Liu, C., Tan, G., Qing, Z., Yang, S., Yang, J., Tan, Y., Yang, R., 2016. Biosens. Bioelectron. 77, 673–680.
Stone, M.D., Mihalusova, M., O'Connor, C.M., Prathapam, R., Collins, K., Zhuang, X., 2007. Nature 446, 458.
Tian, T., Peng, S., Xiao, H., Zhang, X., Guo, S., Wang, S., Zhou, X., Liu, S., Zhou, X., 2013. Chem. Commun. 49, 2652–2654.
Wang, D., Guo, R., Wei, Y., Zhang, Y., Zhao, X., Xu, Z., 2018. Biosens. Bioelectron. 122, 247–253.
Wang, L., Chen, C., Huang, H., Huang, D., Luo, F., Qiu, B., Guo, L., Lin, Z., Yang, H., 2018. Biosens. Bioelectron. 121, 153–158.
Wang, L., Meng, T., Fan, Y., Chen, C., Guo, Z., Wang, H., Zhang, Y., 2018. J. Colloid Interface Sci. 524, 1–7.
Wang, L., Meng, T., Jia, H., Feng, Y., Gong, T., Wang, H., Zhang, Y., 2019. J. Colloid Interface Sci. 549, 98–104.
Wang, L., Meng, T., Liang, L., Sun, J., Wu, S., Wang, H., Yang, X., Zhang, Y., 2019. Sens. Actuators, B 278, 133–139.
Wang, L., Meng, T., Yu, G., Wu, S., Sun, J., Jia, H., Wang, H., Yang, X., Zhang, Y., 2019. Biosens. Bioelectron. 124–125, 53–58.
Wang, L., Teng, Q., Sun, X., Chen, Y., Wang, Y., Wang, H., Zhang, Y., 2018. J. Colloid Interface Sci. 512, 127–133.
Wang, L.J., Ma, F., Tang, B., Zhang, C.Y., 2016. Chem. Sci. 8, 2495–2502.
Wu, L., Wang, J., Ren, J., Qu, X., 2014. Adv. Funct. Mater. 24, 2727–2733.
Xu, X., Wei, M., Liu, Y., Liu, X., Wei, W., Zhang, Y., Liu, S., 2017. Biosens. Bioelectron. 87, 600–606.
Xu, Y., 2011. Chem. Soc. Rev. 40, 2719–2740.
Yan, Z., Li-Juan, W., Chun-Yang, Z., 2014. Chem. Commun. 50, 1909–1911.
Yang, H., Liu, A., Wei, M., Liu, Y., Lv, B., Wei, W., Zhang, Y., Liu, S., 2017. Anal. Chem. 89, 12094–12100.
Yang, W., Zhu, X., Liu, Q., Lin, Z., Qiu, B., Chen, G., 2011. Chem. Commun. 47, 3129–3131.
Yang, X.-J., Zhang, K., Zhang, T.-T., Xu, J.-J., Chen, H.-Y., 2017. Anal. Chem. 89, 4216–4222.
Yang, X., Liu, X., Liu, Z., Pu, F., Ren, J., Qu, X., 2012. Adv. Mater. 24, 2890–2895.
Yi, Z., Wang, H.B., Chen, K., Gao, Q., Tang, H., Yu, R.Q., Chu, X., 2014. Biosens. Bioelectron. 53, 310–315.
Zhang, H.-R., Wang, Y.-Z., Wu, M.-S., Feng, Q.-M., Shi, H.-W., Chen, H.-Y., Xu, J.-J., 2014. Chem. Commun. 50, 12575–12577.
Zhang, H.-R., Wu, M.-S., Xu, J.-J., Chen, H.-Y., 2014. Anal. Chem. 86, 3834–3840.
Zhang, L., Zhang, S., Pan, W., Liang, Q., Song, X., 2016. Biosens. Bioelectron. 77, 144–148.
Zhang, Y., Bo, X., Nsabimana, A., Munyentwali, A., Han, C., Li, M., Guo, L., 2015. Biosens. Bioelectron. 66, 191–197.
Zhou, X., Xing, D., 2012. Chem. Soc. Rev. 41, 4643–4656.
Zhu, X., Ye, H., Liu, J.-W., Yu, R.-Q., Jiang, J.-H., 2018. Anal. Chem. 90, 13188–13192.
Zhuang, Y., Shang, C., Lou, X., Xia, F., 2017. Anal. Chem. 89, 2073–2079.